Angular and energy distributions of secondary electrons from helium. Slow electrons ejected by electron impact

Yong-Ki Kim*
Argonne National Laboratory, Argonne, Illinois 60439 and Joint Institute for Laboratory Astrophysics, University of Colorado and National Bureau of Standards, Boulder, Colorado 80309
(Received 7 February 1983)

Recommended angular and energy distributions of slow secondary electrons produced from helium by electron impact are presented in a compact table. The table lists coefficients for the Legendre polynomials from which all angular and energy distributions can be generated for scattering angles between 0° and 180°, secondary-electron energies between 0 and 40 eV, and incident-electron energies between 100 and 2000 eV. The distributions represent double-differential cross sections that are consistent with expected asymptotic behavior, angular symmetry, and integrated cross sections. These cross sections should be sufficiently reliable to serve as normalization standards for experiments on secondary-electron distributions.

I. INTRODUCTION

Angular and energy distributions of electrons ejected from atoms and molecules by energetic photons and charged particles play important roles in the study of energy deposition and the subsequent generation of collision products by such projectiles. These distributions also serve as a sensitive means of comparing theory and experiment.

For electron-impact ionization, scattered electrons cannot be distinguished from ejected electrons. Therefore, for convenience, the slower of the two electrons that emerge after an ionizing collision is called the secondary electron and the faster one the primary electron. This operational definition limits the maximum energy of a secondary electron to one half of the kinetic energy to be shared by the two electrons. In the present work, we shall not consider multiple ionization resulting from a single collision. In helium, single ionization is dominant over double ionization.

Although the pioneering work of Mohr and Nicoll[1] was reported in 1934, many experimental papers on secondary electrons ejected by electron impact[2–7] and proton impact[8,9] have been published in the last two decades. These experiments measure cross sections for the production of secondary electrons without detecting primary electrons in coincidence. Also, theoretical studies of the subject, mostly in the first Born approximate have been recently reported.[9–11] Secondary-electron distributions are characterized by three continuous variables, i.e., the angle of ejection θ, the kinetic energy W of the secondary electron, and the incident energy T of the projectile. In reality, however, experiments are carried out only for selected, discrete values of T, and the resulting cross sections are commonly called double-differential cross section (DDCS), differential in W and θ. Practical limitations also restrict measurements of DDCS to certain combinations of the variables W and θ (measured from the incident beam direction), while applications of such cross sections to other branches of physics, e.g., radiation physics and astrophysics, require the continuous dependence of the DDCS on these variables. Moreover, existing experimental and theoretical cross sections on secondary electrons are fragmentary and often disagree with each other. They are sometimes laced with systematic distortions peculiar to the experimental or theoretical methods used. The purpose of this work is to present a consistent set of DDCS for helium which is continuous in T, W, and θ, and which satisfies known theoretical and experimental requirements on asymptotic and threshold behaviors, angular symmetry, and integrated cross sections.

The recommended cross sections do not depend on any specific theory or experiment; they are based on the Born cross sections at high T but, at lower T, they follow the shape of experimental angular and incident-energy dependences which have been modified to meet known requirements. The Legendre polynomials of order 0 to 6 have been fitted to the recommended cross sections for six values of W (0—40 eV) and six values of T (100—2000 eV) to describe the angular and energy distributions in the form

$$\frac{d^2\sigma(T)}{dW\,d\Omega_s} = \sum_{n=0}^{6} A_n(T,W)P_n(\cos\theta)\ , \tag{1}$$

where $d\Omega_s = 2\pi d(\cos\theta)$ is the solid-angle element of the seondary electron, P_n is the nth-order Legendre polynomial, and A_n is the corresponding fitted coefficient. With a table of A_n, which is presented later, one can generate and interpolate DDCS to any combination of θ (0°—180°), W, and T within the ranges covered. The table of A_n is compact compared to the DDCS tables that have been previously published.

Although the secondary-electron energies treated here, $W = 0$—40 eV, are limited in scope, they represent the majority of ejected electrons produced by electron-impact ionization of atoms and molecules. Furthermore, existing experimental data show signs of inconsistency for secondary electrons with $W < 10$ eV. The adopted angular distribution at $W = 0$ follows the Born cross sections calculated by Bell and Kingston[10] in shape but not in magnitude. The magnitude was determined through consistency

requirements, which will be described later. No direct measurement of the angular distribution at $W=0$ is available.

The recommended cross sections have been thoroughly checked for consistency with integrated cross sections which, in turn, must satisfy their own experimental and theoretical requirements. The recommended DDCS are meant to represent only gross features of secondary-electron distributions; details such as autoionization peaks (e.g., $2s\,2p\,^1P$) have not been incorporated into the present work. Similar to double ionization, autoionization contributes little (less than 1% in integrated cross sections) compared to single ionization in helium.

Most of the requirements for the electron-impact ionization cross sections also apply to the cross sections for proton-impact ionization. The procedures used in this paper, therefore, will also be useful in determining similar, recommended cross sections for electrons ejected by proton-impact ionization.

In Sec. II, some conventions and graphical methods of analysis are described. In Sec. III, the requirements to be satisfied by the DDCS are summarized, and the procedures used in the determination of the recommended cross sections are explained in Sec. IV. The recommended cross sections are also presented in Sec. IV. Existing experimental and theoretical results are compared with the recommended cross sections in Sec. V, and the conclusions are presented in Sec. VI.

II. CONVENTIONS AND GRAPHICAL METHODS OF ANALYSIS

For the determination and comparison of the DDCS, it is convenient to scale the cross sections by the corresponding Rutherford cross sections instead of using the DDCS directly. The original Rutherford cross section[12] is the single-differential cross section (SDCS) for the ejection of one electron initially at rest (i.e., free)

$$\frac{d\sigma_{\text{free}}}{dW}=\frac{4\pi a_0^2}{T}\frac{R^2}{W^2}\ , \tag{2}$$

where $a_0=0.529$ Å is the Bohr radius and $R=13.6$ eV is the Rydberg energy. Unfortunately, the free-electron Rutherford cross section diverges when the ejected-electron energy diminishes, in clear contradiction with theoretical predictions[13] and experimental evidence.[14] The secondary-electron energy dependence W^{-2} in Eq. (2) resulted from converting K^{-4}, where K is the momentum transferred to the target atom during the collision, into the kinetic energy of the ejected electron, treating it as a free electron. For the ejection of a bound electron, however, part of the momentum transfer must be used to overcome the binding energy B of the electron. Therefore, for the ionization of a bound electron, we use the energy transfer

$$E=W+B \tag{3}$$

instead of W in Eq. (2):

$$\frac{d\sigma_R}{dE}=\frac{4\pi a_0^2}{T}\frac{R^2}{E^2}\ . \tag{4}$$

Equation (4) is referred to as the modified Rutherford cross section.[15] Note that Eq. (4) reduces to Eq. (2) for very fast secondary electrons, i.e., when $W\gg B$.

The scaling of SDCS and DDCS by the modified Rutherford cross section is equivalent to expressing the cross sections in terms of an effective number of free electrons in the target.

The SDCS $d\sigma(T)/dW$ is obtained by integrating DDCS Eq. (1), over the secondary-electron angles

$$\frac{d\sigma(T)}{dW}\equiv\int\frac{d^2\sigma(T)}{dW\,d\Omega_s}d\Omega_s\ . \tag{5}$$

Then, the scaled SDCS

$$Y(T,W)\equiv\frac{d\sigma(T)}{dW}\Big/\frac{d\sigma_R}{dE}=\frac{d\sigma(T)}{dW}\frac{T}{4\pi a_0^2}\frac{E^2}{R^2} \tag{6}$$

for He approaches two as the ejected-electron energy increases (see Fig. 1). Note that the scaled SDCS, $Y(T,W)$, is dimensionless, and we have the advantage that its magnitude stays within one or two decades while the actual cross section varies over many decades. Similarly, the scaled DDCS $Z(T,W,\theta)$, is defined by

$$Z(T,W,\theta)=\frac{d^2\sigma}{dW\,d\Omega_s}\Big/\frac{d\sigma_R}{dE}=\frac{d^2\sigma}{dW\,d\Omega_s}\frac{T}{4\pi a_0^2}\frac{E^2}{R^2}\ . \tag{7}$$

The scaled DDCS has the dimension of steradian^{-1}, and has the physical meaning of effective number of secondary electrons ejected into the solid-angle element $d\Omega_s$.

There are two graphical methods that are well suited in

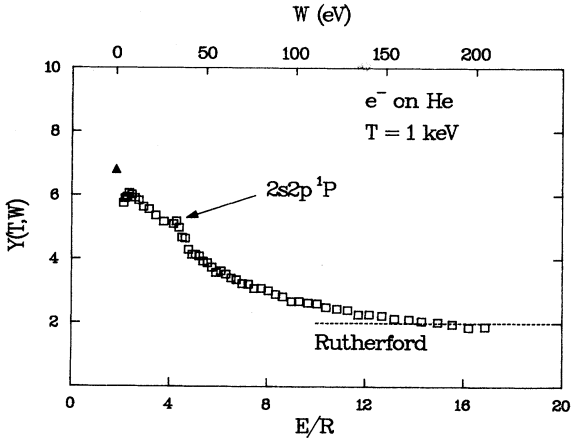

FIG. 1. Scaled single-differential cross section for the ionization of He by 1-keV electrons. Scaled cross section $Y(T,W)$ defined by Eq. (6) represents the effective number of free electrons in the target. Energy transfer in Rydbergs E/R is defined by Eq. (3). Kinetic energy of secondary electrons W is given by the top scale, and T is the incident energy. Open squares represent the experimental data by Opal *et al.* (Ref. 2). Solid triangle is the theoretical cross section obtained by extrapolating Born cross sections for discrete excitations to the ionization limit (Ref. 13). Dashed line marked Rutherford corresponds to the modified Rutherford cross section [Eq. (4)] for two free electrons. Small peak near $W=35$ eV results from the autoionization of the doubly excited state $2s\,2p\,^1P$. Sharp bend below $W\sim 6$ eV in the experimental data is probably due to poor collection efficiency of slow electrons.

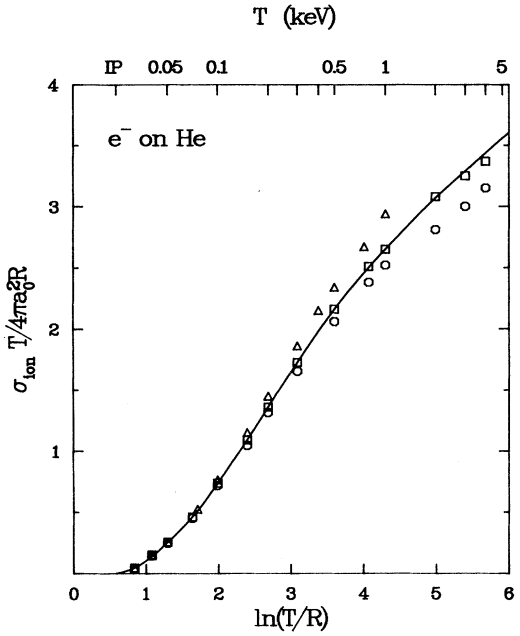

FIG. 2. Fano plot of the recommended cross section for the ionization of He by electron impact σ_{ion}. Solid curve represents the recommended cross section which is based on the experimental data by Smith (Ref. 24, squares) for $T \leq 2$ keV and on the Born cross section (Ref. 25) for $T > 2$ keV. Circles represent σ_{ion} recommended by de Heer and Jansen (Ref. 27) and the triangles represent σ_{ion} measured by Rapp and Englander-Golden (Ref. 26).

elucidating various properties of electron-impact cross sections. The first one is known as the Fano plot,[16] where the scaled cross section [Eq. (6)] is plotted as a function of $\ln(T/R)$. This presentation is based on the asymptotic (high-T) behavior of the Born cross sections[16,17]

$$\sigma_{\text{Born}} \simeq \frac{4\pi a_0^2}{T/R}\left[A \ln\left[\frac{T}{R}\right]+B\right], \tag{8}$$

where A and B, known as the Bethe parameters, are constants that depend on the properties of the target atom but not on the projectile or incident energy. Moreover, the first Bethe parameter A is directly related to the dipole oscillator strength f

$$A=\frac{f}{E/R}, \tag{9}$$

where E is now the photon energy needed to cause excitations of interest. Equations (8) and (9) are general features of the Born approximation and have been verified in numerous examples of discrete excitations and ionizing collisions.[16] The Fano plot can be used for all types of cross sections, e.g., the total ionization cross section, the SDCS, or the DDCS.

One can use the collision strength, defined as $\sigma T/\pi a_0 R$, as the ordinate of the Fano plot instead of the scaled cross section Y defined by Eq. (6). In either case, the plotted quantity should approach, at high T, a straight line with a plot of $4A$ (if the collision strength is used) or $AE^2/R^2=fE/R$ (if the scaled cross section is used). The relevant dipole oscillator strength f can be obtained from

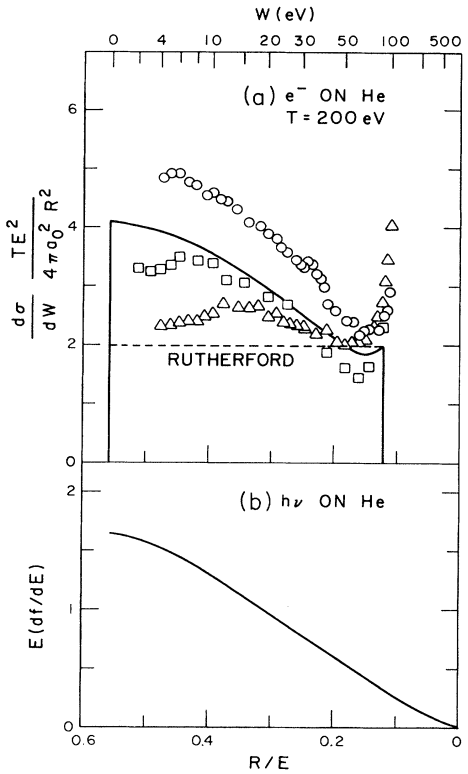

FIG. 3. Platzman plot of single-differential cross sections for ionization of He for (a) ionization by 200-eV electrons and (b) photoionization. Bottom scale is the inverse of the energy transfer in Rydbergs E/R which is also photon energy. Ordinate of (a) is the scaled SDCS defined by Eq. (6). Solid curve in (a) is the recommended SDCS (Fig. 10 and Ref. 18) with appropriate boundaries for the secondary-electron energy W. Area bounded by the solid curve is proportional to σ_{ion} at $T=200$ eV [Eq. (10)]. As was done in Fig. 1, the dashed line marked Rutherford represents the cross section for two free electrons without the electron-exchange effect. Shape of the SDCS above the Rutherford cross section closely follows the shape of the dipole interaction, which is represented by the dipole oscillator strength df/dE, shown in a dimensionless form [Eqs. (9) and (15)] in (b). Adopted dipole oscillator strength is based on the experimental data in Refs. 20–22. Circles denote electron-impact data by Opal *et al.* (Ref. 2), the squares represent those by Shyn and Sharp (Ref. 6), and the triangles stand for those by Rudd and DuBois (Ref. 4). $2s2p\,^1P$ autoionization peak is seen near $W=35$ eV in the data by Opal *et al.* Minimum near $W=65$ eV in (a) is a manifestation of the electron-exchange effect.

experiments or calculations on photoabsorption and photoionization, which, in most cases, are known better than the cross sections for electron- and proton-impact excitations and ionizations. An example of the Fano plot is shown in Fig. 2 for the total ionization cross section σ_{ion} of He by electron impact. The solid curve in Fig. 2 represents the ionization cross section to which the SDCS have been normalized.[18] As will be explained later, accurate SDCS are needed to normalize the angular distribution.

The other graphical method is known as the Platzman

plot,[15] where the scaled SDCS $Y(T,W)$ are plotted as functions of the inverse of the energy transfer E defined by Eq. (3). Figure 3(a) is a typical example. The Platzman plot demonstrates that the effective number of free electrons participating in ionizing collisions approaches the number of valence electrons in the target as the secondary-electron energy is increased. Also, the Platzman plot amplifies details such as the autoionization peaks, the Cooper minimum, the electron-exchange effect, and the similarity to the photoionization cross sections that are difficult to identify in conventional log-log plots of secondary-electron energy distributions. For instance, the portion of the scaled cross section for He presented in Fig. 3(a) for low W ($<$ 50 eV) resembles the *shape* of the corresponding photoionization cross section [Fig. 3(b)] superimposed on the Rutherford cross section for two free electrons; i.e., the dashed line in Fig. 3(a). This resemblance between the photoionization cross section and the SDCS is a manifestation of the relationship given in Eqs. (8) and (9) predicted by the Born approximation at high incident energies.

By choosing R/E instead of E/R in the Platzman plot, as is done in Fig. 3(a), the area under the scaled cross-section curve bounded by appropriate limits of R/E becomes proportional to the total ionization cross section $\sigma_{\rm ion}$:

$$\int Y(T,W)d(R/E)=\sigma_{\rm ion}(T)\frac{T}{4\pi a_0^2 R} \tag{10}$$

from definitions (3) and (6), where $\sigma_{\rm ion}$ is defined by

$$\sigma_{\rm ion}(T)\equiv\int\frac{d\sigma(T)}{dW}dW\ . \tag{11}$$

The choice of R/E as the abscissa also has an advantage that the abscissa is confined to a well-defined range (between R/B and 0) even for energetic secondary electrons. Also, with the R/E abscissa, the details near the threshold ($W=0$) are amplified, whereas the details for high W($>$200 eV) are squeezed into a narrow region. This choice of abscissa emphasizes that most of the ionizing events are accompanied by the production of slow secondary electrons.

III. REQUIREMENTS FOR DOUBLE-DIFFERENTIAL CROSS SECTIONS

There are six major requirements to be satisfied by double-differential cross sections.

A. Threshold behavior

The first requirement is trivial; cross sections must vanish at the appropriate thresholds. This simple requirement serves as a decisive guide in determining the magnitude of cross sections at low T($<$300 eV).

B. Asymptotic (high-T) behavior of DDCS

The second requirement is the relationship between photoionization cross sections and high incident-energy behavior of secondary-electron cross sections mentioned in Sec. II. This requirement is elucidated through the Born approximation,[16,17] and it is essential in determining the overall shape of the T dependence.

TABLE I. Dipole oscillator strengths for the ionization of He.

W (eV)	E (eV)	$E(df/dE)$
0	24.59	1.645
2	26.59	1.615
4	28.59	1.545
10	34.59	1.275
20	44.59	0.968
40	64.59	0.635

When DDCS are presented in Fano plots, i.e., as functions of $\ln(T/R)$ at fixed values of θ and W, the limiting slopes must be proportional to the oscillator strengths for the angular distribution of photoionized electrons. It is well known[19] that the angular distribution of electrons ejected by unpolarized photons has the general form

$$\sigma_{\rm ph}(E,\theta)=\frac{\sigma(E)}{4\pi}[1-\tfrac{1}{2}\beta(E)P_2(\cos\theta)]\ , \tag{12}$$

where E is the photon energy, $\sigma(E)$ is the integrated photoionization cross section, β is the asymmetry parameter, and P_2 is the second-order Legendre polynomial. Since the dipole oscillator strength f is directly proportional to $\sigma(E)$, we can use Eq. (12) in Eq. (9) with $\sigma(E)$ replaced by f. For photoionization, one must use a differential oscillator strength df/dE, i.e., dipole oscillator strength per unit energy of the photon. Moreover, $\beta=2$ for all E if the electron is ejected from a closed s orbital (in nonrelativistic theory), thus simplifying Eq. (12) to

$$\left.\frac{df(E,\theta)}{dE}\right|_{\rm He}=\frac{df(E)/dE}{4\pi}\tfrac{3}{2}\sin^2\theta\ . \tag{13}$$

By combining Eqs. (7)—(9) with (13), we get the asymptotic (high-T) form of the scaled DDCS

$$Z(T,W,\theta)\simeq(E/R)^2[A(E,\theta)\ln(T/R)+B(E,\theta)]\ , \tag{14}$$

where

$$\left[\frac{E}{R}\right]^2 A(E,\theta)=E\frac{df(E)}{dE}\frac{3}{8\pi}\sin^2\theta \tag{15}$$

for He. Accurate experimental values of $\sigma(E)$ for He, which can be converted to $df(E)/dE$, are available in the literature.[20–22] These values, combined with Eqs. (3), (6)—(9), and (14), completely specify the asymptotic slope of the Fano plot for a given θ and W. For electron-impact ionization, the energy transfer E [Eq. (3)] is equivalent to photon energy. Table I lists the values of $E\,df(E)/dE$, the dimensionless quantity we have used for the slopes in the Fano plot at $W=0$—40 eV. The shape and magnitude of $E(df/dE)$ for He are shown in Fig. 3(b).

C. Angular symmetry in the slope of the Fano plot

The third requirement is the angular symmetry expected in DDCS at high T. The photoelectron angular distribution [Eq. (12)] is an even function of $\cos\theta$, and hence leads to the same value of $\sigma_{\rm ph}(E,\theta)$ at θ_1 and θ_2 such that $\theta_1+\theta_2=180°$. This in turn requires that the slopes of the Fano plot at the two supplementary angles θ_1 and θ_2 (but at the same W value) be equal at high T. This is a subtle constraint on the angular distribution that can identify

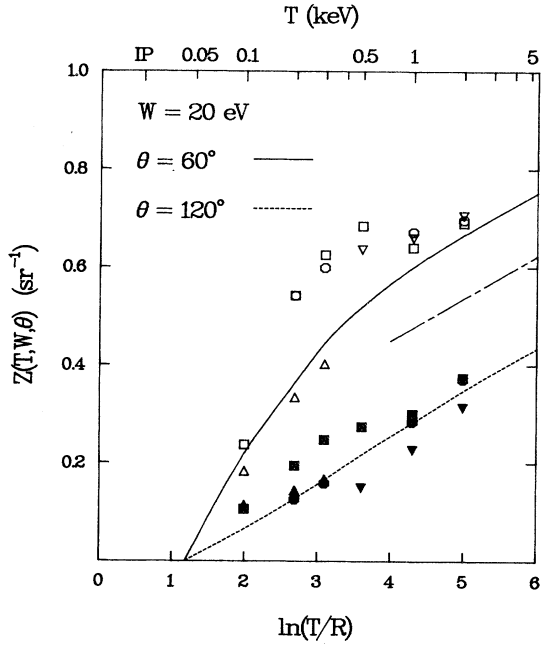

FIG. 4. Fano plot of DDCS for the secondary-electron energy $W=20$ eV at the supplementary angles $\theta=60°$ and 120°. Incident energy is denoted by T, and the Rydberg energy by R. Solid and dashed curves are recommended cross sections, and the dash-dotted line indicates the asymptotic (high-T) slope derived from the photoionization data in Fig. 3. Open symbols are for $\theta=60°$, and the filled ones for 120°. Circles represent the Born cross sections calculated by Bell and Kingston (Ref. 10), and the inverted triangles those by Burnett *et al.* (Ref. 27). Squares are the experimental data by Opal *et al.* (Ref. 2), and the triangles stand for those by Shyn and Sharp (Ref. 6). Ionization potential of He (24.59 eV) is marked IP on the top scale. Cross section must vanish at $T_0=\mathrm{IP}+W$, and for high T, it must have parallel asymptotic slopes at supplementary angles.

systematic distortions in experimental angular distribution. Unfortunately, only the experiment by Beaty *et al.*[2,3] used incident energies high enough to bring out the asymptotic properties predicted by the Born theory. As was reported earlier,[23] the experimental data by Beaty *et al.* showed expected forward-backward symmetries in most cases. An example of this angular symmetry is shown in Fig. 4.

D. Integrated cross sections

The requirement that the angular distribution should yield the correct integrated cross section appears trivial, but it is an important constraint for the renormalization of DDCS. Both types of integrated cross sections SDCS and σ_{ion} must exhibit appropriate slopes when presented in the Fano plot; the slopes are determined from corresponding oscillator strengths for photoionization, $df(E)/dE$, the values of which are well known. Moreover, SDCS must connect smoothly with corresponding cross sections for discrete excitations through the following relationship based on the quantum-defect theory[13]

$$\lim_{n\to\infty}\frac{(n^*)^3}{2}\sigma_n(T)=\left.\frac{d\sigma(T)}{dW/R}\right|_{W=0}, \tag{16}$$

where n^* is the effective principal quantum number of discrete states and σ_n is the sum of all discrete-excitation cross sections with the same principal quantum number n that corresponds to n^*.

A direct measurement of $d\sigma/dW$ is difficult, but Grissom *et al.*[14] measured $d\sigma/dW$ for T up to 500 eV in the special case of $W=0$. In addition, of course, $d\sigma/dW$, when integrated over W, must yield correct σ_{ion}. As was mentioned earlier, the area in the Platzman plot is directly proportional to σ_{ion}, and hence the values of σ_{ion} provide a basis for the renormalization of $d\sigma/dW$. We have adopted the σ_{ion} measured by Smith[24] for $T\lesssim 2$ keV and the Born cross section for higher T.[25] The more recent measurement of σ_{ion} by Rapp and Englander-Golden[26] and σ_{ion} adopted by de Heer and Jansen[27] are not consistent with the asymptotic behavior predicted by theory.[25] The adopted σ_{ion} is presented in Fig. 2 and compared with these experimental data.[24–27]

E. Energy-loss cross section and $d\sigma/dW$

For targets with a single shell, such as hydrogen and helium, the SCDS must match the energy-loss cross section of the incident electron, because there is a unique correspondence between the ejected electron and the incident electron, if double ionization and double excitation are ignored. This is a powerful constraint on $d\sigma/dW$, but it will not help to determine angular distribution because they are very different for primary and secondary electrons. The angular distribution of secondary electrons is spread out to all angles, whereas that of primary electrons is sharply peaked in the forward direction.

F. Binary peak

Qualitatively, secondary electrons are ejected by a combination of glancing (large impact parameters) and knock-on (small impact parameters) collisions. Glancing collisions exhibit characteristics dominated by the dipole interaction, which leads to an angular distribution given by Eq. (12), i.e., symmetric with respect to $\theta=90°$, with a maximum or minimum at $\theta=90°$ depending on the value of β. Knock-on collisions, on the other hand, are dominated by binary collisions, i.e., billiard-ball collisions. From energy and momentum conservation, one can easily derive the relationship between the angle of ejection θ_b, incident energy, and ejected-electron energy if the target electron is unbound and at rest and the electron-exchange effect is ignored,

$$\cos\theta_b\,|_{\mathrm{free}}=\sqrt{W/T}\ . \tag{17}$$

Again, we should replace W by E [Eq. (3)] for the same reason that we used E in Eq. (4) for a bound electron,

$$\cos\theta_b\,|_{\mathrm{bound}}\cong\sqrt{E/T}\ . \tag{18}$$

In reality, the binary peak is spread out due to the momentum distribution of the bound electron. The actual position of the binary peak depends on the interference between glancing and knock-on collisions, but Eq. (18) serves as a *qualitative* guideline, placing the binary peak some-

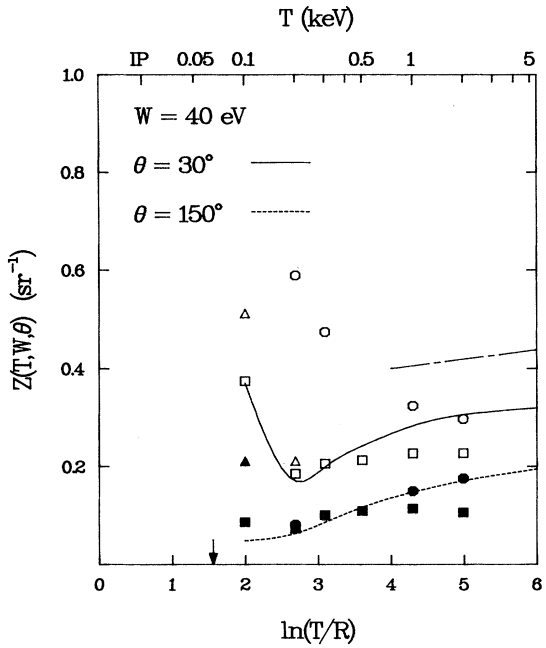

FIG. 5. Fano plot of DDCS for the secondary-electron energy $W=40$ eV at the supplementary angles $\theta=30°$ and 150°. Legend is the same as in Fig. 4, except for the triangles, which represent the experimental data by Rudd and DuBois (Ref. 4). Arrow near $\ln(T/R)=1.6$ indicates the minimum value of T needed to eject an electron with $W=40$ eV. Cross section for $T=100$ eV peaks in the forward direction since an electron with 40-eV kinetic energy is a primary electron. Note that the data by Opal *et al.* (Ref. 2) would be too low when their data at $T=200$, 300, and 500 eV are reduced by about 20% (see Fig. 4).

where between $\theta=45°$ ($E\sim T/2$) and 90° ($E\ll T$). Electrons that belong to the "recoil" peak in triple-differential cross sections[28] contribute to the backward ($\theta>90°$) intensity in DDCS.

IV. RECOMMENDED CROSS SECTIONS

The recommended cross sections were determined through an iterative process in which the DDCS have been scrutinized for consistency in one variable, while others were kept constant. For instance, scaled DDCS at a given θ and W were put in the Fano plot to check their T dependence. The values chosen for explicit determination of the DDCS are $T=100$, 200, 300, 500, 1000, and 2000 eV; $W=0$, 2, 4, 10, 20, and 40 eV, and for θ, every 15° between 0° and 180°.

As starting values, we used the Born cross sections at $T=2$ keV calculated by Bell and Kingston.[10] The initial values of the DDCS at lower T were determined by following the shape of the T dependence of the experimental data by Beaty and co-workers,[2,3] while keeping in mind that all cross sections must vanish at the appropriate thresholds; i.e., at

$$T_0(W)=W+B\ . \tag{19}$$

In addition, the asymptotic slopes of the Fano plots were required to match corresponding values, which were de-

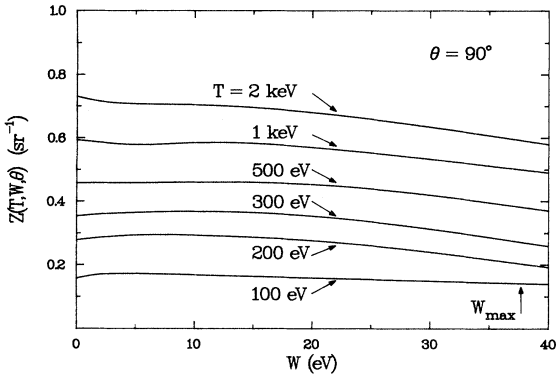

FIG. 6. Scaled DDCS at the ejection angle $\theta=90°$ as functions of the secondary-electron energy W and incident-electron energy T. Arrow marked W_{max} is the maximum value of W for $T=100$ eV [Eq. (20)].

rived from photoionization data (see Table I.) Since the dipole-allowed component is always present in ionization, various Fano plots will show a monotonic increase as T is increased due to the $\ln T$ term in Eq. (8). An exception is for $W=40$ eV, $T=100$ eV, and in forward angles, where the angular distribution begins to peak forward because an electron of 40-eV kinetic energy is a primary electron, not a secondary electron (see Fig. 5).

After this was done for the selected values of θ, the DDCS were integrated over the secondary-electron solid angle Ω_s to be compared with the SDCS values. Actually, the integration over Ω_s was carried out indirectly by first fitting the angular distribution (for fixed values of T and W) to the Legendre polynomials [see Eq. (1)]. Then, only P_0 in Eq. (1) survives after the integration over Ω_s, leading to a simple relationship

$$d\sigma/dW=4\pi A_0\ . \tag{20}$$

The angular distribution was renormalized by scaling all A_n's so that the integrated cross section agrees with the SDCS values determined earlier[18] through appropriate consistency checks.

The renormalized DDCS were then plotted as functions of W at fixed values of T and θ. Except for the region near $W=35$ eV where autoionization peaks are expected, the DDCS of He should show a smooth (but not necessarily monotonic) W dependence. An example of DDCS vs W plot is shown in Fig. 6. The DDCS thus adjusted were iterated again through the procedures described above, until they showed expected consistency and asymptotic behavior in all variables.

The angular distributions thus determined are expressed in terms of the Legendre polynomials [Eq. (1)], and Table II lists the fitted values of A_n for the selected values of T and W. In Table II, five significant figures are provided, though they are not physically meaningful, to make interpolation reliable to three significant figures. Examples of the recommended DDCS are presented in Figs. 7–9 in units of the modified Rutherford cross sections [Eq. (4)]. The recommended SDCS determined earlier[18] are reproduced as a Platzman plot in Fig. 10 for convenience.

Owing to the smooth behavior of σ_{ion}, SDCS, and the

TABLE II. Legendre polynomial coefficients for the recommended double-differential cross sections [Eq. (1)]. The FORTRAN notation is used, e.g., $5.4335E-01 = 5.4335\times10^{-1}$. (Unit: $10^{24}\ m^2/\text{eV sr}$.)

T (eV)	A_0	A_1	A_2	A_3	A_4	A_5	A_6
			$W=0$ eV				
1.0000E+02	2.4315E+01	−3.6178E+00	1.3461E+01	9.4947E−01	−1.0825E+00	−1.7267E+00	5.4335E−01
2.0000E+02	1.7481E+01	−1.5644E+00	4.4725E+00	−1.4262E−01	−4.8146E−01	−5.6169E−01	9.4022E−02
3.0000E+02	1.3620E+01	−9.0697E−01	1.6229E+00	−4.0871E−01	−2.0550E−01	−1.7046E−01	3.5876E−02
5.0000E+02	9.7183E+00	−4.8485E−01	−2.5285E−01	−3.5363E−01	3.3389E−02	1.8768E−02	−3.4207E−02
1.0000E+03	5.8352E+00	−2.1791E−01	−9.8456E−01	−1.8451E−01	1.1498E−01	2.0016E−02	−7.4009E−02
2.0000E+03	3.4148E+00	−8.8496E−02	−9.6801E−01	−1.1795E−01	7.1730E−02	2.9427E−02	−3.3555E−02
			$W=2$ eV				
T (eV)	A_0	A_1	A_2	A_3	A_4	A_5	A_6
1.0000E+0.2	2.0152E+01	3.4006E+00	8.7238E+00	−1.0847E+00	4.7903E−01	7.3401E−01	8.7892E−01
2.0000E+02	1.4740E+01	1.8978E+00	2.7815E+00	−1.4254E+00	−7.6945E−02	2.2538E−01	3.4064E−01
3.0000E+02	1.1525E+01	1.3363E+00	8.0986E−01	−1.3193E+00	6.5648E−03	1.5080E−01	1.5384E−01
5.0000E+02	8.1663E+00	7.9443E−01	−4.8194E−01	−9.0454E−01	1.1996E−01	1.1060E−02	2.7343E−03
1.0000E+03	4.9080E+00	3.6697E−01	−9.4358E−01	−4.8787E−01	7.2150E−02	−5.5097E−03	1.2968E−02
2.0000E+03	2.8557E+00	1.7766E−01	−8.4539E−01	−2.6354E−01	5.1012E−02	−6.2407E−03	1.1644E−03
			$W=4$ eV				
T (eV)	A_0	A_1	A_2	A_3	A_4	A_5	A_6
1.0000E+02	1.6540E+01	4.7853E+00	5.6784E+00	−2.2915E+00	9.4870E−02	1.6852E−01	−7.5955E−02
2.0000E+02	1.2454E+01	2.8626E+00	1.5449E+00	−2.0992E+00	−2.9720E−02	2.1870E−01	4.8854E−02
3.0000E+02	9.7403E+00	1.9741E+00	1.7181E−01	−1.7141E+00	6.4167E−02	2.2304E−01	1.1381E−02
5.0000E+02	6.9264E+00	1.1914E+00	−6.4104E−01	−1.1680E+00	1.2860E−01	9.3615E−02	−4.6242E−02
1.0000E+03	4.1449E+00	5.5822E−01	−9.0017E−01	−6.3769E−01	9.5135E−02	4.8509E−02	2.2843E−02
2.0000E+03	2.4117E+00	2.7228E−01	−7.6270E−01	−3.3544E−01	8.2050E−02	2.1826E−02	−7.0487E−03
			$W=10$ eV				
T (eV)	A_0	A_1	A_2	A_3	A_4	A_5	A_6
1.0000E+02	9.5613E+00	3.9717E+00	8.9789E−01	−3.5379E+00	−3.9068E−01	−3.7655E−01	−6.3390E−01
2.0000E+02	7.6829E+00	2.7020E+00	−5.0487E−01	−2.6872E+00	−7.3428E−02	−8.5395E−03	−2.4694E−01
3.0000E+02	6.1479E+00	2.0037E+00	−8.9029E−01	−2.1316E+00	1.3362E−01	1.1728E−01	−1.4251E−01
5.0000E+02	4.4065E+00	1.2497E+00	−1.0070E+00	−1.3655E+00	2.1648E−01	1.3575E−01	−7.3756E−02
1.0000E+03	2.6581E+00	6.4202E−01	−8.6969E−01	−7.2215E−01	2.0985E−01	9.2173E−02	−4.6736E−02
2.0000E+03	1.5410E+00	3.2067E−01	−6.2309E−01	−3.6339E−01	1.4628E−01	5.4663E−02	−3.3768E−02

TABLE II. (*Continued.*)

T (eV)	A_0	A_1	A_2	A_3	A_4	A_5	A_6
			$W=20$ eV				
1.0000E+02	4.5003E+00	2.2215E+00	−1.3139E+00	−3.0103E+00	3.1511E−01	9.4256E−01	2.5693E−01
2.0000E+02	3.8478E+00	1.7254E+00	−1.3110E+00	−2.3030E+00	2.4161E−01	7.1576E−01	2.1827E−01
3.0000E+02	3.1950E+00	1.3445E+00	−1.2399E+00	−1.8220E+00	2.6739E−01	5.6017E−01	1.7290E−01
5.0000E+02	2.3557E+00	8.8913E−01	−1.0285E+00	−1.1753E+00	2.9786E−01	3.4213E−01	4.2996E−02
1.0000E+03	1.4292E+00	4.7972E−01	−6.9499E−01	−6.0918E−01	2.2020E−01	1.5910E−01	−2.4284E−02
2.0000E+03	8.2688E−01	2.4713E−01	−4.4453E−01	−2.9992E−01	1.4321E−01	6.6537E−02	−3.5761E−02
			$W=40$ eV				
1.0000E+02	2.5000E+00	3.0960E+00	1.2755E+00	−5.0855E−01	−9.2720E−02	4.2599E−03	6.5672E−02
2.0000E+02	1.3698E+00	1.0719E+00	−5.9411E−01	−1.3443E+00	−2.5644E−01	3.2904E−01	2.2371E−01
3.0000E+02	1.1388E+00	7.9882E−01	−5.5770E−01	−1.0265E+00	−8.5447E−02	2.7986E−01	1.1823E−01
5.0000E+02	8.8713E−01	5.3342E−01	−5.0648E−01	−6.9070E−01	5.4731E−02	1.9031E−01	3.1001E−02
1.0000E+03	5.5031E−01	2.7944E−01	−3.4967E−01	−3.5456E−01	8.7722E−02	9.3639E−02	−8.5212E−03
2.0000E+03	3.1512E−01	1.3852E−01	−2.1666E−01	−1.7555E−01	6.7121E−02	4.5694E−02	−1.3226E−02

DDCS of He, which was attained partly by ignoring autoionization peaks, one can interpolate the DDCS reconstructed from Eq. (1) and Table II to any combination of T, W, and θ, within the ranges covered in Table II. We have verified that DDCS, for numerous interpolated values of W, yield SDCS consistent with those presented in Fig. 10, although $d\sigma/dW$ can be directly interpolated from Table II by using Eq. (20). The interpolation in T should be carried out by using the Fano plots for each W and θ (e.g., Figs. 4 and 5), whereas the interpolation in W should be done by using graphs of the type shown in Fig. 6. The cubic spline interpolation in DDCS, not in A_n's, is recommended for these interpolations.

A word of caution is warranted, however, for *extrapolating* the DDCS beyond the ranges covered in Table II. For instance, although a cubic-spline method is excellent for interpolation, we have found that the extrapolation of Table II to $W=50$ eV by a straightforward quadratic fit works better than a cubic-spline method. Extrapolation of Table II in W beyond 50 eV is not recommended.

The extrapolation of Table II to high T is more complicated. First of all, as a consequence of relativistic kinematics, one must use $\ln[\beta^2/(1-\beta^2)]-\beta^2$ instead of $\ln(T/R)$ in all Fano plots for $T>5$ keV.[16] Secondly, a linear extrapolation is required after each Fano plot reaches expected asymptotic behavior. If the extrapolation in T is done judiciously, in combination with Table I to provide proper asymptotic slopes, Table II can easily be extended to cover a wide range of T values to hundreds of keV.

V. COMPARISON WITH OTHER DATA

None of the theoretical and experimental data available in the literature cover all the values of θ, W, and T that can be generated from Table II nor agree fully with the recommended DDCS. For instance, the recommended DDCS for $W=0$ closely follow the angular distribution calculated by Bell and Kingston[10] for high T, but their values at higher W and lower T tend to be too large, particularly in forward angles. The Born cross sections calcu-

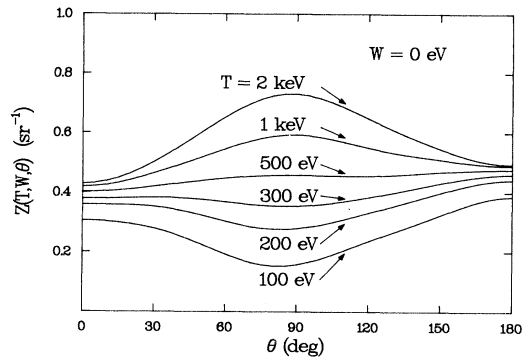

FIG. 7. Recommended DDCS scaled by the Rutherford cross sections [Eq. (7)] for the secondary-electron energy $W=0$ as functions of the ejection angle θ and the incident-electron energy T. In the scaled unit, the ordinate represents the effective number of free electrons ejected into a unit solid angle at θ. Shape of a scaled angular distribution at a given T, however, is the same as that of an unscaled cross section.

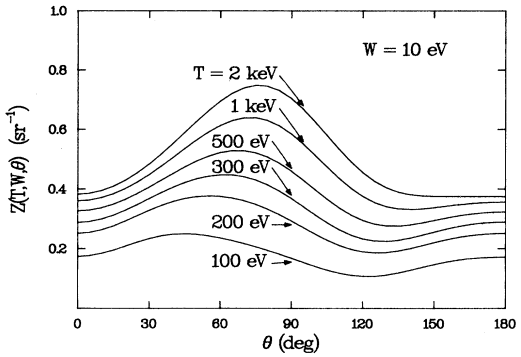

FIG. 8. Same as Fig. 7 for the secondary-electron energy $W=10$ eV.

lated by Burnett *et al.*[29] are of comparable quality as those by Bell and Kingston. Both calculations used correlated initial- and final-state target wave functions. Some of their theoretical data at $W=20$ eV are compared with the recommended DDCS in Fig. 4. In general, the data by Burnett *et al.* tend to have higher maxima and lower minima than those calculated by Bell and Kingston and also all experimental data quoted in the present work. We have followed experimental shapes in the backward direction because there are less experimental problems there and experimental data are judged more reliable there than in the forward direction. The Born cross sections by Bell and Kingston shown in Figs. 4 and 5 are much higher than the recommended cross sections at low T. This trend of high cross sections at low T is inherent in the Born theory for most electron-impact cross sections.

As is clear from Fig. 4, the data by Opal *et al.*[2] at $T=200$, 300, and 500 eV should be reduced by about 20% to make them consistent with their own data at $T=100$, 1000, and 2000 eV. This is also evident in Fig. 3 for the integrated cross section.

A notable discrepancy between the recommended DDCS and the experiments by Rudd and DuBois[4] and by Shyn and Sharp[6] is a sharp peak in the forward direction ($\theta \lesssim 15°$) that they have reported but is absent from our

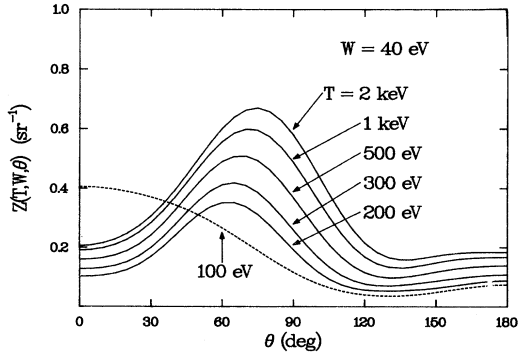

FIG. 9. Same as Fig. 7 for the secondary-electron energy $W=40$ eV. Cross section for $T=100$ eV is given by the dashed curve to indicate that a 40-eV electron is a primary electron.

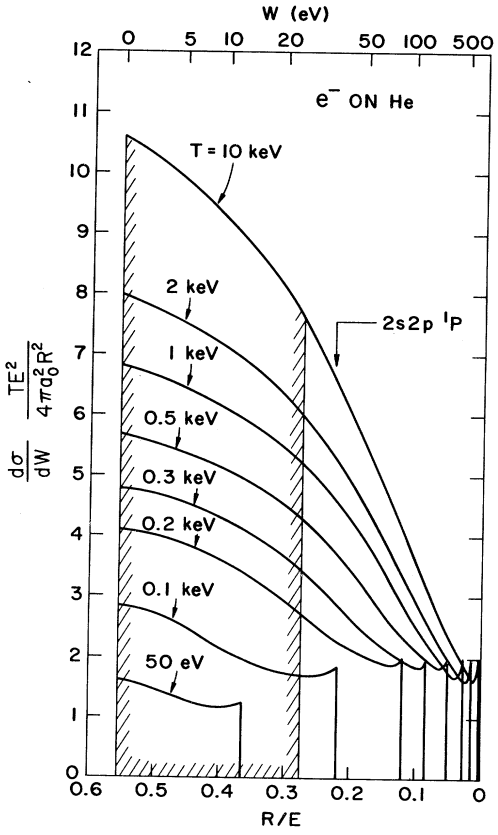

FIG. 10. Platzman plot of the recommended SDCS scaled by the modified Rutherford cross sections [Eq. (4)] as functions of incident energy T (reproduced from Ref. 18). Secondary-electron energy W is given by the top scale. Shaded area represents the fraction of secondary electrons ejected with $W \leq 24.59$ eV that are too slow to ionize in subsequent collisions in a dense He target. Fraction shown here for He, roughly $\frac{2}{3}$ or more, is typical of many atoms and molecules (Refs. 15 and 18).

recommended cross section. An example of the discrepancy is shown in Fig. 11. At $W=20$ eV and $T=200$ eV, the binary peak is well developed as indicated by all three sets of experimental data shown in the figure. Moreover, the experimental binary peaks are all in the neighborhood of $\theta_b=62°$ given by Eq. (18). Yet, the experimental data from Refs. 4 and 6 show a sharp rise in the extreme forward direction. Although suggestions have been put forward to attribute the peak to the electron-exchange effect,[4,5] there is no plausible theory that supports the existence of such an exchange peak. In fact, Oda and Nishimura[30] studied the peak in detail, but finally concluded that the peak was an experimental artifact.

Compared to our DDCS, the experimental angular distribution by Rudd and DuBois[4] as well as that by Shyn and Sharp[6] is sometimes too high in the backward direction ($\theta > 90°$) and too low in the forward angles ($\theta < 90°$) except for the sharp peak in the extreme forward direction. All experimental data in the backward direction, however, show far smoother angular distributions than the data in the forward direction. This probably is associated with low background noise in the backward direction,

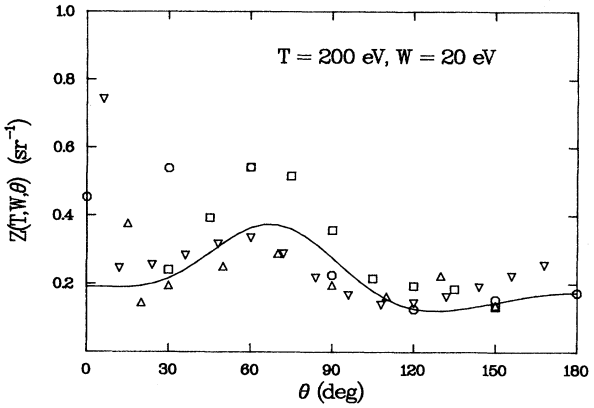

FIG. 11. Comparison of the angular distributions for $T=200$ eV and $W=20$ eV. Solid curve is the recommended cross section, the circles are the Born cross section calculated by Bell and Kingston (Ref. 10), the squares are the experimental data by Opal *et al.* (Ref. 2), the triangles are those by Rudd and DuBois (Ref. 4), and the inverted triangles are those by Shyn and Sharp (Ref. 6). Sharp peak at $\theta < 20°$ reported in Refs. 4 and 6 are likely to be an experimental artifact.

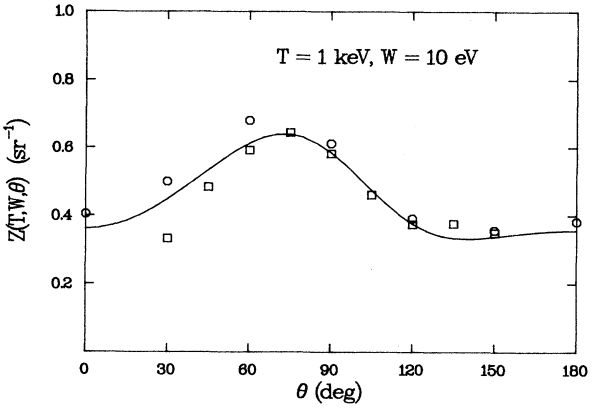

FIG. 12. Same as Fig. 11 for $T=1$ keV and $W=10$ eV. Trend observed in the Born cross section by Burnett *et al.* (Ref. 29, not shown here), indicates that their cross section would lie substantially below the recommended cross section for $\theta > 120°$.

while high noise level is expected in the forward direction due to the presence of the incident beam as well as elastically scattered electrons.

As was pointed out in Refs. 4 and 6, the experimental values at $\theta=30°$ and 150° by Opal *et al.*[2] tend to be too low. This is borne out in Figs. 5 and 11. As was mentioned earlier, the data by Opal *et al.* at $T=200$ eV should be reduced by about 20%. This renormalization will bring the Opal data in Fig. 11 into good agreement with the recommended DDCS, except for the values at $\theta=30°$ and 150°, which are too low. The same trend is observed in most of the data by Opal *et al.*,[2] although their data at $T=1$ and 2 keV agree much better with theory[10] and the present work, as is shown in Fig. 12.

All experimental values shown in this paper are subject to 20—30% combined uncertainties. It is difficult, however, to include these uncertainties directly in applications, such as energy degradation modeling, because the systematic part of the uncertainties will influence the outcome in a complicated manner. Although the recommended DDCS, in principle, cannot be more accurate than the original theoretical and experimental data that they are based on, we hope that the enforcement of consistency requirements would have corrected most of the "systematic" uncertainties associated with experiment and theory.

VI. CONCLUDING REMARKS

We have assembled a recommended set of double-differential cross sections for the ionization of He by electron impact. This recommendation is based on experimental and theoretical data not only on the DDCS but also on integrated and photoionization cross sections. Although the range of the secondary-electron energy that has been covered in this work is limited to $W \leq 40$ eV, the recommended DDCS should be useful in modeling studies, since these slow secondary electrons include more than $\frac{3}{4}$ of all ionizing events in He (see Fig. 10). The recommended cross sections are presented in terms of the coefficients for the Legendre polynomials, A_n [see Eq. (1)]. These coefficients are listed in a compact table (Table II) from which the DDCS for any combination of θ, W, and T such that $0° \leq \theta \leq 180°$, $0 \leq W \leq 40$ eV, and $100 \leq T \leq 2000$ eV can be interpolated. Along with total ionization and single-differential cross sections (Figs. 2 and 10), the present work will provide a mutually consistent mapping of cross sections for electron-impact ionization. These cross sections are suitable as input for various applications that require a complete and consistent set of collision data.

To make the DDCS presented here more complete, one should add the angular distribution of autoionization peaks near $W=35$ eV. Since these peaks are sharp, however, experimental data are sensitive to the energy resolution of the instruments used. For instance, the data in Ref. 2 have several points (in W) which cover the autoionizing region (Figs. 1 and 3), but such an energy grid is too coarse to provide a full understanding of the autoionization peaks. The doubly excited states of He are subjects of many current studies.[31] Few of these, however, provide the information on absolute cross sections that is needed for our purpose.

With minor modifications, procedures used in the present work can be extended: (a) to higher values of W and T on the ionization of He by electron impact, (b) to the determination of consistent DDCS for the ionization of He by proton impact, and (c) to the ionization of other atoms and molecules by both electron and proton impact.

As was shown in Secs. III and IV, the T dependence of the DDCS plays a crucial part in determining a consistent set of cross sections. In this respect, experimental data that cover a wide range of T such as those by Opal, Beaty, and Peterson[2] are most valuable in applying consistency checks. Other types of experimental data potentially useful in completing the mapping of DDCS are those for $T < 100$ eV, angular distribution (absolute cross sections) of autoionized electrons, and the DDCS for fast secondary electrons near

$$W_{\max}=(T-B)/2\ , \tag{21}$$

where the electron-exchange effect is expected to be large. In fact, the so-called $(e,2e)$ experiments can easily be modified (by shutting down one of the electron detectors) to provide the DDCS near $W_{\max}$, as was done by van Wingerden *et al.*[32] For atoms and molecules with many inner shells, data on multiple ionization are necessary to interpret the DDCS properly.

Finally, we hope that the DDCS proposed here will stimulate further experimental and theoretical work on He to verify the details of the recommended cross sections. We also hope the recommended DDCS will serve as a normalization standard for measurements of electron-impact ionization cross sections on other atoms and molecules.

ACKNOWLEDGMENTS

This work was initiated while the author was visiting the Joint Institute for Laboratory Astrophysics (JILA), and he is grateful for the hospitality extended by the JILA staff, particularly to Dr. J. Gallagher and her staff of the JILA Atomic Collision Cross Section Data Center. He is indebted to Dr. E. C. Beaty, Dr. R. D. DuBois, Professor N. Oda, Professor M. E. Rudd, and Dr. T. W. Shyn for extensive discussions and unpublished data provided to him on numerous occasions during the last decade. He also thanks Professor U. Fano and Professor S. T. Manson for helpful comments on the manuscript. This work was supported by the U.S. Department of Energy and the Office of National Standard Reference Data System, National Bureau of Standards.

*Permanent address: Argonne National Laboratory, Argonne, Illinois 60439.

[1]C. B. O. Mohr and F. H. Nicoll, Proc. R. Soc. London, Ser. A 144, 596 (1934).
[2]C. B. Opal, E. C. Beaty, and W. K. Peterson, At. Data Nucl. Data Tables 4, 209 (1972).
[3]E. C. Beaty, Radiat. Res. 64, 70 (1975), and references therein.
[4]M. E. Rudd and R. D. DuBois, Phys. Rev. A 16, 26 (1977), and references therein.
[5]N. Oda, Radiat. Res. 64, 80 (1975), and references therein.
[6]T. W. Shyn and W. E. Sharp, Phys. Rev. A 19, 557 (1979).
[7]T. W. Shyn, W. E. Sharp, and Y.-K. Kim, Phys. Rev. A 24, 79 (1981), and references therein.
[8]M. E. Rudd, L. H. Toburen, and N. Stolterfoht, At. Data Nucl. Data Tables 18, 413 (1976), and references therein.
[9]L. H. Toburen, S. T. Manson, and Y.-K. Kim, Phys. Rev. A 17, 148 (1978), and references therein.
[10]K. L. Bell and A. E. Kingston, J. Phys. B 8, 2666 (1975), and references therein.
[11]D. H. Madison, Phys. Rev. A 8, 2449 (1973), and references therein.
[12]For instance, see L. Landau and E. M. Lifshitz, *Quantum Mechanics, Nonrelativistic Theory* (Pergamon, London, 1965), 2nd ed., p. 575.
[13]Y.-K. Kim and M. Inokuti, Phys. Rev. A 7, 1257 (1973).
[14]J. T. Grissom, R. N. Compton, and W. R. Garrett, Phys. Rev. A 6, 977 (1972).
[15]Y.-K. Kim, Radiat. Res. 61, 21 (1975).
[16]M. Inokuti, Rev. Mod. Phys. 43, 297 (1971); M. Inokuti, Y. Itikawa, and J. E. Turner, *ibid.* 50, 23 (1978).
[17]H. A. Bethe, Ann. Phys. (Leipzig) 5, 325 (1930).
[18]Y.-K. Kim, Radiat. Res. 64, 205 (1975).
[19]D. J. Kennedy and S. T. Manson, Phys. Rev. A 5, 227 (1972).
[20]J. A. R. Samson, Adv. At. Mol. Phys. 2, 177 (1966).
[21]J. B. West and G. V. Marr, Proc. R. Soc. London, Ser. A 349, 397 (1976).
[22]J. Berkowitz, *Photoabsorption, Photoionization, and Photoelectron Spectroscopy* (Academic, New York, 1979), p. 75.
[23]Y.-K. Kim, Phys. Rev. A 6, 666 (1972).
[24]P. T. Smith, Phys. Rev. 36, 1293 (1930).
[25]Y.-K. Kim and M. Inokuti, Phys. Rev. A 3, 665 (1971).
[26]D. Rapp and P. Englander-Golden, J. Chem. Phys. 43, 1464 (1965).
[27]F. J. de Heer and R. H. J. Jansen, J. Phys. B 10, 3741 (1977).
[28]H. Ehrhardt, M. Fischer, and K. Jung, Z. Phys. A 304, 119 (1982).
[29]T. Burnett, S. P. Rountree, G. Doolen, and W. D. Robb, Phys. Rev. A 13, 626 (1976).
[30]N. Oda and F. Nishimura, in *Abstracts of the Tenth International Conference on the Physics of Electronic and Atomic Collisions, Paris, 1977,* edited by M. Barat and J. Reinhardt (Commissariat à L'Énergie Atomique, Paris, 1977), p. 362.
[31]For instance, see A. Pochat, R. J. Tweed, M. Doritch, and J. Peresse, J. Phys. B 15, 2269 (1982), and references therein.
[32]B. van Wingerden, J. T. N. Kimman, M. van Tilberg, and F. J. de Heer, J. Phys. B 14, 2475 (1981).